

Enhanced nonlinear damping in graphene by parametric-direct internal resonance

Ata Keşkekler*,¹ Oriel Shoshani,² Herre S. J. van der Zant,³ Peter G. Steeneken,^{1,3} and Farbod Alijani*¹

¹*Department of Precision and Microsystems Engineering, TU Delft, The Netherlands*

²*Department of Mechanical Engineering, Ben-Gurion University of Negev, Israel*

³*Kavli Institute of Nanoscience, TU Delft, The Netherlands*

(Dated: September 7, 2022)

Nonlinearities are ubiquitous in nanomechanical systems. They manifest themselves already at low vibration amplitudes, alter the stiffness and unlock energy decay paths through intermodal couplings. Although strong nonlinear stiffness variations have been observed in nanomechanical systems, to date, their nonlinear damping is conceived to be a fixed parameter, independent from the drive level or frequency. In this letter, we experimentally show that nonlinear damping of graphene nanodrum resonators can be strongly enhanced via parametric-direct internal resonance. By regulating the drive level, we tune the parametric resonance of the nanodrum over a large range of 40-70 MHz to reach two-to-one internal resonance, while demonstrating a nearly two-fold increase of the nonlinear damping. We derive an analytical model that captures the observed physics, and provides supporting evidence that nonlinear damping is amplified near internal resonance. Our study opens up an exciting route towards utilizing modal interactions and parametric resonance at nanoscale for realizing resonators with tunable nonlinear damping over wide frequency ranges.

In nature, from macro down to nano scale, dynamical systems evolve towards thermal equilibrium while exchanging energy with their surroundings. Dissipative mechanisms that mediate this equilibration, convert energy from the dynamical system of interest to heat in an environmental bath. The details of this process can be extremely intricate, nonlinear, and in most cases hidden behind the veil of linear viscous damping, which is merely an approximation valid for small amplitude oscillations.

In the last decade, nonlinear damping mechanisms have attracted much attention in the study of nanomechanical resonators. It has been shown that the nonlinear dissipation process in these devices obeys the empirical force model $F_d = -\tau_{nl}x^2\dot{x}$ where τ_{nl} is the nonlinear damping coefficient, x is the displacement and \dot{x} velocity [1]. To date, the microscopic physical mechanism from which this empirical damping force originates has remained ambiguous, with a diverse range of phenomena being held responsible including viscoelasticity [2, 3], phonon-phonon interactions [4], and mode coupling [5, 6]. The fact that nonlinear damping can stem from multiple origins simultaneously, makes isolating one route from the others a daunting task, especially since the nonlinear damping coefficient τ_{nl} is perceived to be a fixed parameter in nanoresonators that, unlike stiffness [7–9], quality factor [10], and nonlinear stiffness [11–13], cannot be tuned easily.

Amongst the different mechanisms that affect nonlinear damping, intermodal coupling is particularly interesting, as it can be enhanced near internal resonance (IR), a special condition at which the ratio of the resonance

frequencies of the coupled modes is a rational number [14]. The internal resonance phenomenon has frequently been observed in nano/micro-mechanical resonators [15–24] because for these systems, vibrations become nonlinear already at small amplitudes. At internal resonance, modes can interact strongly even if their nonlinear coupling is relatively weak. Interestingly, internal resonance is closely related to the effective stiffness of resonance modes, and can therefore be manipulated by careful engineering of the geometry of nanomechanical systems, their spring hardening nonlinearity [25], and electrostatic spring softening [24].

Here, we demonstrate that nonlinear damping of graphene nanodrums can be strongly enhanced by parametric-direct internal resonance. To achieve this, we bring the fundamental mode of the nanodrum into parametric resonance, allowing it to be tuned over a wide frequency range from 40-70 MHz. We extract the nonlinear damping as a function of the parametric drive level, and observe that it increases as much as 80 % when the frequency shift of the parametric resonance brings it into internal resonance with a higher mode. By comparing the characteristic dependence of the nonlinear damping coefficient on parametric drive to a theoretical model, we confirm that internal resonance can be held accountable for the significant increase in nonlinear damping.

Experiments are performed on a 10 nm thick multilayer graphene nanodrum with a diameter of 5 μm , that is transferred over a cavity etched in a layer of SiO_2 with a depth of 285 nm. We use a power modulated blue laser ($\lambda = 488 \text{ nm}$) to thermomechanically actuate the nanodrum. We then read-out the motion using a red laser ($\lambda = 633 \text{ nm}$) whose reflected intensity is modulated by the motion of the nanodrum in a Fabry-Pérot etalon formed by the graphene and the Si back mirror (Fig. 1a). The reflected red laser intensity from the cen-

*Corresponding authors:

Ata Keşkekler <a.keskekler-1@tudelft.nl>

Farbod Alijani <f.alijani@tudelft.nl>

ter of the drum is detected using a photodiode, whose response is read by the same Vector Network Analyzer (VNA) that modulates the blue laser. The measured VNA signal is then converted to displacement in nanometers using a nonlinear optical calibration method [26] (see Supplemental Material [27] I).

By sweeping the drive frequency we obtain the frequency response of the nanodrum in which multiple directly driven resonance modes can be identified (Fig. 1b). We find the fundamental axisymmetric mode of vibration at $f_{0,1}=20.1$ MHz and several other modes, of which the two modes, at $f_{2,1}^{(1)}=47.4$ MHz and $f_{2,1}^{(2)}=50.0$ MHz, are of particular interest. This is because, to study the effect of internal resonance on nonlinear damping, we aim to achieve a two-to one (2:1) internal resonance by parametrically driving the fundamental mode, such that it coincides with one of the higher frequency modes. The frequency ratios $f_{2,1}^{(1)}/f_{0,1} \approx 2.3$ and $f_{2,1}^{(2)}/f_{0,1} \approx 2.4$ are close to the factor 2, however additional frequency tuning is needed to reach the 2:1 internal resonance condition.

The parametric resonance can be clearly observed by modulating the tension of the nanodrum at frequency ω_F with the blue laser while using a frequency converter in the VNA to measure the amplitude at $\omega_F/2$ as shown in Fig. 1c. By increasing the parametric drive, we observe a Duffing-type geometric nonlinearity over a large frequency range, such that the parametrically driven fundamental resonance can be tuned across successive 2:1 internal resonance conditions with modes $f_{2,1}^{(1)}$ and $f_{2,1}^{(2)}$, respectively.

In Fig. 1c we observe that the parametric resonance curves (upward driving frequency sweeps) follow a common response until they reach the saddle-node bifurcation frequency f_{SNB} above which the parametric resonance curve reaches its peak amplitude A_{SNB} and drops down to low amplitude. We note that the value of A_{SNB} can be used to determine the degree of nonlinear damping, because it is very sensitive to τ_{nl1} in a Duffing-van der Pol-Mathieu oscillator [28]. To extract the nonlinear damping coefficient τ_{nl1} of mode $f_{0,1}$ from the curves in Fig. 1c, we use the following single degree-of-freedom (DoF) model to describe the system dynamics:

$$\ddot{x}_1 + \omega_1^2 x_1 + \gamma x^3 = F_1 x_1 \cos(\omega_F t) - 2\tau_1 \dot{x}_1 - 2\tau_{\text{nl1}} x_1^2 \dot{x}_1, \quad (1)$$

in which $\omega_1 = 2\pi f_{0,1}$ is the eigenfrequency of the axisymmetric mode of the nanodrum, γ is its Duffing constant and F_1 and ω_F are the parametric drive amplitude and frequency, respectively. Moreover, $2\tau_1 = \omega_1/Q$ is the linear damping coefficient, with Q being the quality factor, and τ_{nl1} is the nonlinear damping term of van der Pol type that prevents the parametric resonance amplitude A_{SNB} from increasing to infinity [28, 29] at higher driving frequencies since $|A_{\text{SNB}}|^2 \propto (2F_1 Q - 4)/\tau_{\text{nl1}}$.

To identify the parameters governing the device dynamics from the measurements in Fig. 1c, we use Eq. (1)

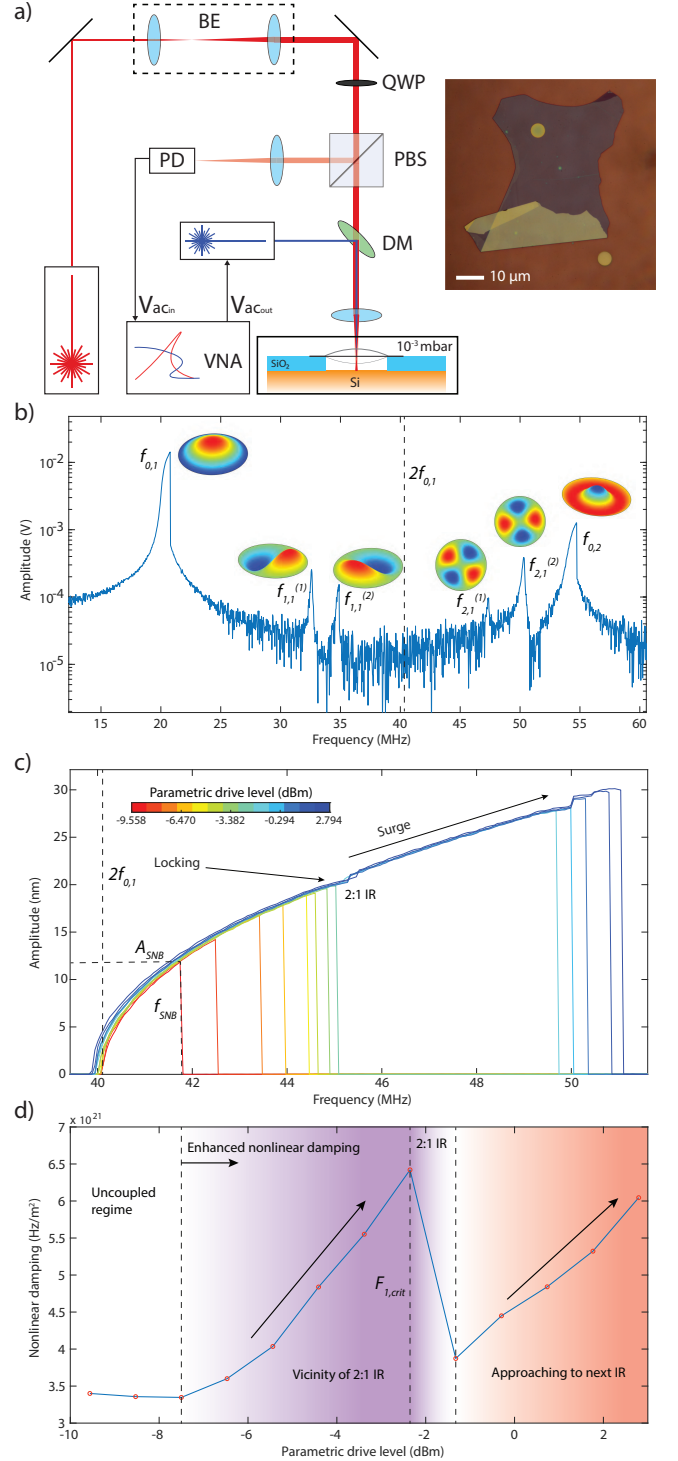


FIG. 1: Nonlinear dynamic response of a graphene nanodrum near 2:1 internal resonance. (a) Fabry-Pérot interferometry with thermomechanical actuation and microscope image of the graphene. Experiments are performed in vacuum at 10^{-3} mbar. In the figure; BE: Beam expander, QWP: Quarter wave plate, PBS: Polarized beam splitter, PD: Photodiode, DM: Dichroic mirror, VNA: Vector network analyzer. (b) Direct frequency response curve of the device, showing multiple resonances (Drive level = -12.6 dBm). The mode shapes are simulated by Comsol. (c) Parametric resonance curves, driven at twice the detection frequency. (d) Variation of the nonlinear damping τ_{nl1} as a function of drive F_1 .

and obtain good fits of the parametric resonance curves using τ_{nl1} and γ as fit parameters (details of the fits can be found in Supplemental Material [27] IV). The linear quality factor Q of the resonator is determined at low drive level to be 454 and has been fixed throughout the fitting procedure. The numerical error in determining τ_{nl1} from the fits is typically $< 0.1\%$ (see Fig. 4 in Supplemental Material [27]).

As we gradually increase the drive level, f_{SNB} increases until it reaches the vicinity of the internal resonance, where we observe an increase in τ_{nl1} (Fig. 1d). Whereas f_{SNB} increases with parametric drive F_1 , Fig. 1c shows that its rate of increase $\frac{df_{\text{SNB}}}{dF_1}$ slows down close to $f_{2,1}^{(1)}$, locking the saddle-node-bifurcation frequency when $f_{\text{SNB}} \approx 45$ MHz. At the same time, τ_{nl1} increases significantly at the associated parametric drive levels, providing the possibility to tune nonlinear damping up to two-folds by controlling F_1 , as seen in Fig. 1d.

Fig. 1c also shows that above a certain critical parametric drive level $F_{1,\text{crit}}$, the frequency locking barrier at $f_{\text{SNB}} \approx 45$ MHz is broken and f_{SNB} suddenly jumps to a higher frequency (≈ 5 MHz higher), and a corresponding larger A_{SNB} . We label this increase in the rate $\frac{df_{\text{SNB}}}{dF_1}$ by “surge” in Fig. 1c, where an abrupt increase in the amplitude-frequency response is observed to occur above a critical drive level $F_{1,\text{crit}}$. Interestingly, even above $F_{1,\text{crit}}$ a further increase in τ_{nl1} is observed with increasing drive amplitude, indicating that a similar frequency-locking occurs when the parametric resonance peak reaches the second internal resonance at $f_{\text{SNB}} \approx f_{2,1}^{(2)}$.

Although the 1 DoF model in Eq. (1) can capture the response of the parametric resonance, it can only do so by introducing a drive level dependent nonlinear damping coefficient $\tau_{\text{nl1}}(F_1)$ (Fig. 1d). To study the physical origin of this drive level dependent nonlinear damping, we extend the model by introducing a second mode whose motion is described by generalized coordinate x_2 . Moreover, to describe the coupling between the interacting modes at the 2:1 internal resonance, we use the single term coupling potential $U_{\text{cp}} = \alpha x_1^2 x_2$ (see Supplemental Material [27] II for the details). The coupled equations of motion in the presence of this potential become:

$$\begin{aligned} \ddot{x}_1 + \omega_1^2 x_1 + \gamma \dot{x}_1^3 + \frac{\partial U_{\text{cp}}}{\partial x_1} &= F_1 x_1 \cos(\omega_F t) - 2\tau_1 \dot{x}_1 - 2\tau_{\text{nl1}} x_1^2 \dot{x}_1, \\ \ddot{x}_2 + \omega_2^2 x_2 + \frac{\partial U_{\text{cp}}}{\partial x_2} &= F_2 \cos(\omega_F t) - 2\tau_2 \dot{x}_2. \end{aligned} \quad (2)$$

The 2 mode model describes a parametrically driven mode with generalized coordinate x_1 coupled to x_2 that has eigenfrequency $\omega_2 = 2\pi f_{2,1}^{(1)}$, damping ratio τ_2 , and is directly driven by a harmonic force with magnitude F_2 .

To understand the dynamics of the system observed experimentally and described by the model in Eq. (2),

it is convenient to switch to the rotating frame of reference by transforming x_1 and x_2 to complex amplitude form (see Supplemental Material [27] III for the slow dynamic equations). This transformation reveals a system of equations that predicts the response of the resonator as the drive parameters (F_1 , F_2 , and ω_F) are varied. Solving the coupled system at steady-state yields the following algebraic equation for the amplitude a_1 of the first mode:

$$\begin{aligned} \left[\tau_1 + (\tau_{\text{nl1}} + \tilde{\alpha}^2 \tau_2) \frac{a_1^2}{4} \right]^2 + \left[\Delta\omega_1 - \left(\frac{3\gamma}{\omega_F} + \tilde{\alpha}^2 \Delta\omega_2 \right) \frac{a_1^2}{4} \right]^2 \\ = \frac{1}{4\omega_F^2} \left[F_1^2 + \tilde{\alpha}^2 (F_2^2 + 2\omega_F \Delta\omega_2 F_1 F_2 / \alpha) \right], \end{aligned} \quad (3)$$

where $\Delta\omega_1 = \omega_F/2 - \omega_1$ and $\Delta\omega_2 = \omega_F - \omega_2$ are the frequency detuning from the primary and the secondary eigenfrequencies, and $\tilde{\alpha}^2 = \alpha^2 / [\omega_F^2 (\tau_2^2 + \Delta\omega_2^2)]$ is the rescaled coupling strength. Essentially, the first squared term in (3) captures the effect of damping on the parametric resonance amplitude a_1 , the second term captures the effect of nonlinear coupling on the stiffness and driving frequency, and the term on the right side is the effective parametric drive. A set of solutions of this equation is shown in Supplemental Material Fig. 2. From the rescaled coupling strength $\tilde{\alpha}$ and Eq. (3) it can be seen that the coupling $\tilde{\alpha}^2$ shows a large peak close to the 2:1 internal resonance where $|\Delta\omega_2| \approx 0$. Interestingly, this shows that the 2 mode model can account for an increase in the effective nonlinear damping parameter $\tau_{\text{nleff}} = \tau_{\text{nl1}} + \tilde{\alpha}^2 \tau_2$ near internal resonance, in accordance with the observed peak in τ_{nl1} obtained from the experimental fits with the 1 DoF model in Fig. 1d.

The 2 mode model of Eq. (3) allows us to obtain good fits of the parametric resonance curves in Fig. 1b, with a constant $\tau_{\text{nl1}} \approx 3.4 \times 10^{21}$ (Hz/m²) determined far from internal resonance and a single coupling strength $\alpha = 2.2 \times 10^{22}$ (Hz²/m) which intrinsically accounts for the variation of τ_{nleff} near internal resonance. These fits can be found in Supplemental Material [27] V, and demonstrate that the 2 mode model is in agreement with the experiments for constant parameter values, without requiring drive level dependent fit parameters.

To understand the physics associated with the frequency-locking and amplitude-frequency surge, we use the experimentally extracted fit parameters from the 2 mode model and numerically generate parametric resonance curves using Eq. (3) for a large range of drive amplitudes (see Fig. 2a). We see that for small drive levels, an upward frequency sweep will follow the parametric resonance curve and then will lock and jump-down at the first saddle-node bifurcation (SNB1) frequency, that lies close to $f_{\text{SNB}} \approx f_{2,1}^{(1)}$. At higher parametric drive levels, the parametric resonance has a stable path to traverse the internal resonance towards a group of stable states at higher frequencies.

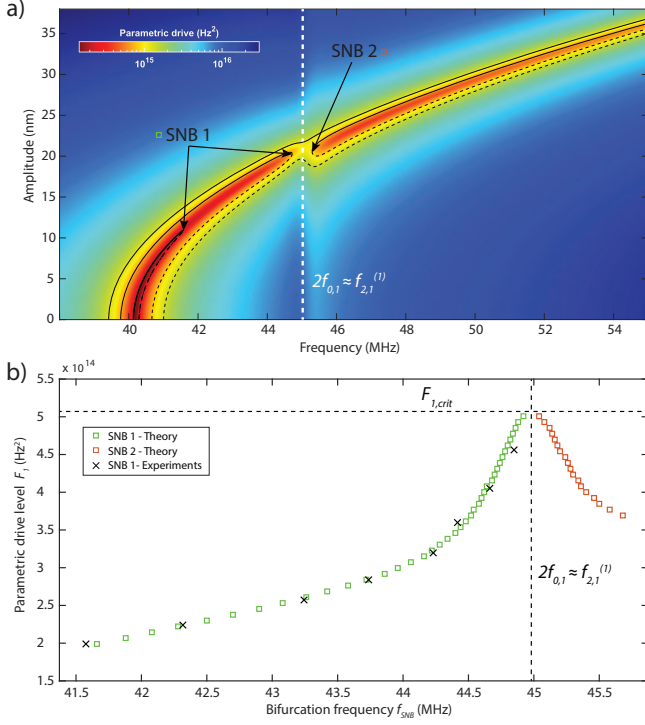


FIG. 2: (a) Color map of the analytical model response curves obtained by using the fitted parameters from experiments. (b) The underlying route of the amplitude-frequency surge is revealed by tracing the evolution of saddle-node bifurcations (SNB1 and SNB2) of the parametric resonance curves.

A more extensive investigation of this phenomenon can be carried out by performing bifurcation analysis of the steady-state solutions (see Supplementary Material [27] III). The bifurcation analysis reveals two saddle-node bifurcations near the singular region of the internal resonance, one at the end of the first path (SNB1) and another at the beginning of the second path (SNB2) (Fig. 2b). As the drive amplitude increases, the saddle-node bifurcation pair starts to move towards each other until they meet and annihilate one another to form a stable solution at the connecting point in a broad frequency range, which we labeled in our experiments as "surge". It is also possible to observe that the rate at which saddle-node pairs approach each other dramatically drops near the internal resonance condition, demonstrating the "locking" which we also observed in the experiments.

To check how closely the 2 mode model captures the variation of the effective nonlinear damping close to the internal resonance condition, we follow a reverse path, and fit the numerically generated resonance curves of Fig. 2a using the 1 DoF model of Eq. (3) with τ_{n11} as the fit parameter. In this way, we track the variation of τ_{n11} in the 1 DoF model with the parametric drive F_1 , similar to what we observed experimentally and reported in Fig. 1c. The result of this fit is shown in Fig. 3a, where a similar

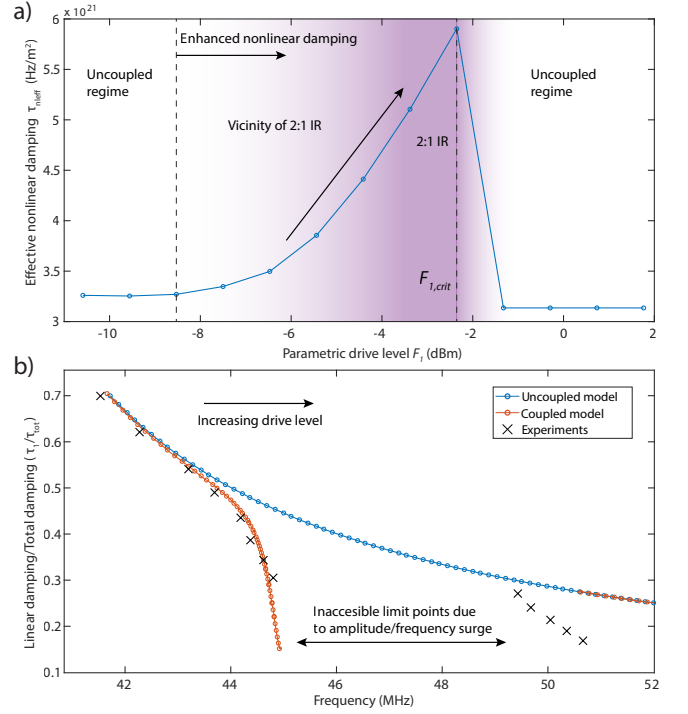


FIG. 3: (a) Variation of the effective nonlinear damping parameter (τ_{nleff}) with respect to parametric drive. The τ_{nleff} is obtained by fitting the numerically generated curves of Fig. 2a as the fit parameter. (b) Comparison of the ratio between linear damping and total damping from experiments and theoretical calculations.

anomalous change of nonlinear damping is obtained for the 2 mode model.

The variation of nonlinear damping affects the total damping (sum of linear and nonlinear dissipation) of the resonator too. It is of interest to study how large this effect is. In Fig. 3b we report the variation in the ratio of the linear damping τ_1 and the amplitude-dependent total damping $\tau_{tot} = (\omega_1/Q + 0.25\tau_{nleff}|x_1|^2)$ [28] in the spectral neighborhood of $f_{2,1}^{(1)}$, and observe a sudden decrease in the total damping is well captured by the 2 mode model. With the increase in the drive amplitude, τ_1/τ_{tot} values of this model though, deviate from those of the experiments due to a subsequent internal resonance at $f_{2,1}^{(2)}/f_{0,1} \approx 2.4$ that is not included in our theoretical analysis. The dependence of τ_1/τ_{tot} on frequency shows that near internal resonance the total damping of the fundamental mode increases nearly by 80%.

When increasing the blue laser power and modulation, the parametrically actuated signal is also observed in the direct detection mode (like in Fig. 1b) due to optical readout nonlinearities [26]. As a result a superposition of Fig. 1b and 1c is obtained, as shown in Fig. 4.

Interestingly, the enhanced laser power increases mem-

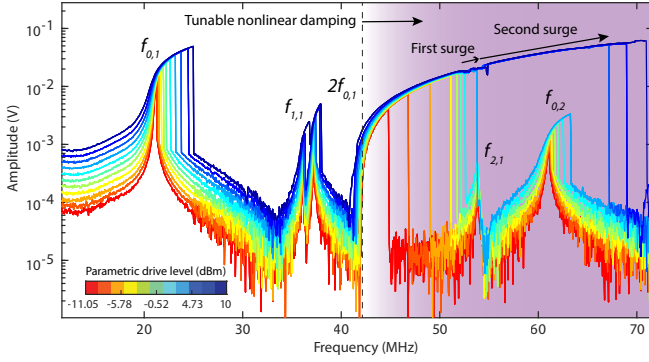


FIG. 4: Frequency response measurements at high drive powers, pushing the parametric resonance response into successive internal resonances. The arrows in the figure show successive amplitude-frequency surges.

brane tension which moves $f_{0,1}$ upward by a few MHz, but also allows us to reach even higher parametric modulation. In this configuration we achieve a frequency shift in f_{SNB} from 40-70 MHz, corresponding to as much as 75 % tuning of the mechanical motion frequency. This large tuning can increase the number of successive internal resonances that can be reached even further, to reach modal interactions between the parametric mode $f_{0,1}$ and direct modes $f_{2,1}^{(2)}$ and $f_{0,2}$ (see Fig. 4). As a result, multiple amplitude-frequency surges can be detected in the large frequency range of 30 MHz over which nonlinear damping coefficient can be tuned.

In summary, we study the tunability of nonlinear damping in a graphene nanomechanical resonator, where the fundamental mode is parametrically driven to interact with a higher mode. When the system is brought near a 2:1 internal resonance, a significant increase in nonlinear damping is observed. In addition, the rate of increase of the parametric resonance frequency reduces in a certain locking regime, stabilizing the values of f_{SNB} and A_{SNB} , which could potentially aid frequency noise reduction [16]. Interestingly, as the drive level is further increased beyond the critical level $F_{1,\text{crit}}$, this locking barrier is broken, resulting in a surge in f_{SNB} and amplitude of the resonator. These phenomena were studied experimentally, and could be accounted for using a 2 mode theoretical model. The described mechanism can isolate and differentiate mode coupling induced nonlinear damping from other dissipation sources. It also provides a way to controllably tune nonlinear damping, which complements existing methods for tuning linear damping [10], linear stiffness [7–9] and nonlinear stiffness [11–13], extending our toolset to adapt and study the rich nonlinear dynamics of nanoresonators.

We thank Martin Lee for fabrication of the cavity substrates and Prof. Marco Amabili for fruitful discussions about nonlinear damping. The research leading to these results received funding from European

Union’s Horizon 2020 research and innovation program under Grant Agreement 802093 (ERC starting grant ENIGMA). O.S. acknowledges support for this work from the United States – Israel Binational Science Foundation under Grant No. 2018041. P.G.S. and H.S.J.v.d.Z. acknowledge funding from the European Union’s Horizon 2020 research and innovation program under grant agreement numbers 785219 and 881603 (Graphene Flagship).

- [1] A. Eichler, J. Moser, J. Chaste, M. Zdrojek, I. Wilson-Rae, and A. Bachtold, *Nature Nanotechnology* **6**, 339 (2011), ISSN 1748-3395.
- [2] S. Zaitsev, O. Shtempluck, E. Buks, and O. Gottlieb, *Nonlinear Dynamics* **67**, 859 (2012), ISSN 1573-269X.
- [3] M. Amabili, *Nonlinear Dynamics* **97**, 1785 (2019), ISSN 1573-269X.
- [4] A. Croy, D. Midtvedt, A. Isacsson, and J. M. Kinaret, *Phys. Rev. B* **86**, 235435 (2012).
- [5] D. Midtvedt, A. Croy, A. Isacsson, Z. Qi, and H. S. Park, *Physical review letters* **112**, 145503 (2014).
- [6] J. Güttinger, A. Noury, P. Weber, A. M. Eriksson, C. Lagoin, J. Moser, C. Eichler, A. Wallraff, A. Isacsson, and A. Bachtold, *Nature nanotechnology* **12**, 631 (2017).
- [7] X. Song, M. Oksanen, M. A. Sillanpää, H. Craighead, J. Parpia, and P. J. Hakonen, *Nano letters* **12**, 198 (2012).
- [8] B. Sajadi, F. Alijani, D. Davidovikj, J. Goosen, P. G. Steeneken, and F. van Keulen, *Journal of Applied Physics* **122**, 234302 (2017).
- [9] M. Lee, D. Davidovikj, B. Sajadi, M. Siskins, F. Alijani, H. S. van der Zant, and P. G. Steeneken, *Nano letters* **19**, 5313 (2019).
- [10] J. M. L. Miller, A. Ansari, D. B. Heinz, Y. Chen, I. B. Flader, D. D. Shin, L. G. Villanueva, and T. W. Kenny, *Applied Physics Reviews* **5**, 041307 (2018).
- [11] P. Weber, J. Guttinger, I. Tsioutsios, D. E. Chang, and A. Bachtold, *Nano letters* **14**, 2854 (2014).
- [12] C. Samanta, N. Arora, and A. Naik, *Applied Physics Letters* **113**, 113101 (2018).
- [13] F. Yang, F. Rochau, J. S. Huber, A. Briessels, G. Rastelli, E. M. Weig, and E. Scheer, *arXiv preprint arXiv:2003.14207* (2020).
- [14] A. H. Nayfeh and D. T. Mook, *Nonlinear Oscillations* (John Wiley & Sons, 1995).
- [15] H. J. R. Westra, M. Poot, H. S. J. van der Zant, and W. J. Venstra, *Phys. Rev. Lett.* **105**, 117205 (2010).
- [16] D. Antonio, D. H. Zanette, and D. López, *Nature communications* **3**, 806 (2012).
- [17] A. Eichler, M. del Álamo Ruiz, J. Plaza, and A. Bachtold, *Physical review letters* **109**, 025503 (2012).
- [18] C. Chen, D. H. Zanette, D. A. Czaplewski, S. Shaw, and D. López, *Nature communications* **8**, 15523 (2017).
- [19] O. Shoshani, S. W. Shaw, and M. I. Dykman, *Scientific reports* **7**, 18091 (2017).
- [20] D. A. Czaplewski, C. Chen, D. Lopez, O. Shoshani, A. M. Eriksson, S. Strachan, and S. W. Shaw, *Physical review letters* **121**, 244302 (2018).
- [21] D. A. Czaplewski, S. Strachan, O. Shoshani, S. W. Shaw,

- and D. López, Applied Physics Letters **114**, 254104 (2019).
- [22] F. Yang, F. Rochau, J. S. Huber, A. Brieussel, G. Rastelli, E. M. Weig, and E. Scheer, Physical review letters **122**, 154301 (2019).
 - [23] S. Hourì, D. Hatanaka, M. Asano, and H. Yamaguchi, Phys. Rev. Applied **13**, 014049 (2020).
 - [24] C. Van der Avoort, R. Van der Hout, J. Bontemps, P. Steeneken, K. Le Phan, R. Fey, J. Hulshof, and J. Van Beek, Journal of Micromechanics and Microengineering **20**, 105012 (2010).
 - [25] H. J. R. Westra, D. M. Karabacak, S. H. Brongersma, M. Crego-Calama, H. S. J. van der Zant, and W. J. Venstra, Phys. Rev. B **84**, 134305 (2011).
 - [26] R. J. Dolleman, D. Davidovikj, H. S. J. van der Zant, and P. G. Steeneken, Applied Physics Letters **111**, 253104 (2017).
 - [27] See Supplemental Material at <http://link.aps.org/>, which includes a description of the measurements calibration, derivation of the equations of motion, model analysis, and model calibration.
 - [28] R. Lifshitz and M. Cross, Review of nonlinear dynamics and complexity **1**, 1 (2008).
 - [29] R. J. Dolleman, S. Hourì, A. Chandrashekar, F. Alijani, H. S. J. van der Zant, and P. G. Steeneken, Scientific Reports **8**, 9366 (2018).